The zonal patterns in late Quaternary South American Monsoon precipitation

T. Kukla[1,2], M. J. Winnick[3], M. M. Laguë[4,5], Z. Xia[3,6]

[1]Department of Geosciences, Colorado State University, Fort Collins, CO, USA
[2]Department of Geological Sciences, Stanford University, Stanford, CA, USA
[3]Department of Geosciences, University of Massachusetts Amherst, Amherst, MA, USA
[4]University of Saskatchewan Coldwater Lab, Canmore, Alberta, Canada
[5]Department of Earth and Planetary Science, University of California Berkeley, Berkeley, CA, USA
[6]School of Geographical Sciences, Northeast Normal University, Changchun, China

Key Points:

- The late Quaternary South American Precipitation Dipole is unlikely due to changes in monsoon strength alone.
- Dipole transitions drive changes in rainfall greater than 1000 mm/yr.
- Spatial monsoon migration explains dipole transitions and reconciles conflicting proxy interpretations.

Corresponding author: Tyler Kukla, `tykukla@colostate.edu`

Abstract

Speleothem oxygen isotope records ($\delta^{18}O$) of tropical South American rainfall in the late Quaternary show a zonal "South American Precipitation Dipole" (SAPD) with wet conditions in the west at the Last Glacial Maximum (LGM; ∼21 ka), in the east at the mid-Holocene (∼7 ka), and in between by the late Holocene (∼1 ka to today). However, the SAPD remains enigmatic because it is expressed differently in western versus eastern $\delta^{18}O$ records and isotope-enabled climate model simulations usually misrepresent the magnitude and/or spatial pattern of $\delta^{18}O$ change. Here, we address the SAPD enigma in two parts. First, we re-interpret the $\delta^{18}O$ data to account for upwind rainout effects which are known to be pervasive in tropical South America, but are not commonly considered in Quaternary paleoclimate studies. Our revised interpretation reconciles the $\delta^{18}O$ data with other hydroclimate proxy records by demonstrating that the amount of rainout is similar in the western and eastern phases of the SAPD (the SAPD is zonally balanced). Second, we hypothesize that the SAPD is driven by the zonal migration of South American Monsoon rainout. Using an energy balance model of monsoon circulation, we find that zonal monsoon migration can be explained by regional energy budget shifts, such as changing Saharan albedo associated with the African Humid Period, that have not been modeled in previous SAPD studies. This zonal monsoon migration hypothesis presents a new framework for interpreting $\delta^{18}O$ records from tropical South America and may help explain the zonal rainfall anomalies that predate the late Quaternary.

Plain Language Summary

Paleoclimate data suggest that, in the last ∼25 thousand years, western Amazonia has been wetter at times when eastern Amazonia is drier, and vice versa. This east-west pattern in past rainfall is known as the "South American Precipitation Dipole", and its extreme western and eastern states approximately coincide with the Last Glacial Maximum (∼21 thousand years ago) and mid-Holocene (∼7 thousand years ago), respectively. However, the cause of the dipole is debated because different models produce different results, and the interpretations of data are in conflict. Central in this conflict are oxygen isotope tracers of past precipitation which show different trends at different sites that are difficult to interpret. We present a new interpretation of these data, backed by model results, which suggests that the precipitation dipole is driven by the monsoon region migrating from west-to-east (and back) across tropical South America. We test this monsoon migration hypothesis with an energy balance climate model which reproduces the expected east-west differences for the Last Glacial Maximum and mid-Holocene. The monsoon migration hypothesis is a possible solution to the precipitation dipole enigma, but the hypothesis remains to be tested in more sophisticated climate models where east-west monsoon migration is less well-studied.

1 Introduction

Tropical South America spans about one-tenth of the Earth's circumference from east to west (zonally). There is mounting evidence that rainfall across this stretch has varied in a zonal "dipole" fashion in the late Quaternary (here, the last ∼25 kyr) with rainfall increasing in northeastern Brazil at the expense of drying in western Amazonia, and vice versa (Martin et al., 1997; Cruz et al., 2009; Cheng et al., 2013). This zonal rainfall pattern is called the "South American Precipitation Dipole" (SAPD), a term that describes the empirical patterns of past rainfall associated with the South American Monsoon, and is distinct from the precipitation dipole studied in modern climate between southeastern South America and the South Atlantic Convergence Zone (Nogués-Paegle & Mo, 1997; Boers et al., 2014). The SAPD has been identified on precession (Martin et al., 1997; Wang et al., 2004; Cruz et al., 2009; Cheng et al., 2013) and glacial-interglacial timescales (Abouchami & Zabel, 2003; Mason et al., 2019), and it corresponds with many high-amplitude signals in paleoclimate proxy data (P. A. Baker, Seltzer, et al., 2001; P. A. Baker, Rigsby, et al., 2001; Tapia et al., 2003; Fritz et al., 2004; Cruz et al., 2009; Wang et al., 2017). Still, conflicting proxy interpretations cast doubt on what drives the SAPD (Cruz et al., 2009; Liu & Battisti, 2015), and even whether it exists at all (Wang et al., 2017).

At the foundation of these conflicting proxy interpretations is an apparent discrepancy between speleothem oxygen isotope records ($\delta^{18}O$) of past rainfall and independent records of continental water runoff (Fig. 1). Specifically, speleothem $\delta^{18}O$ records are zonally imbalanced as trends in the eastern Amazon and northeastern Brazil are twice as large as, and generally the opposite direction of, those to the west. Based on the larger $\delta^{18}O$ shifts in the east, the magnitude of past change in eastern Amazon rainfall should outpace the west (Cruz et al., 2009; Cheng et al., 2013), especially considering that eastern $\delta^{18}O$ is, if anything, less sensitive to precipitation than western $\delta^{18}O$ today (Fig. S1). However, evidence for these seemingly large swings in eastern Amazon rainfall opposes proxy records for continental water runoff—runoff appears to be higher at the Last Glacial Maximum (LGM; $\sim$ 20 ka) when $\delta^{18}O$ is high in the eastern Amazon and northeastern Brazil, and runoff is lower at the mid-Holocene ($\sim$7 ka) when $\delta^{18}O$ is low (Fig. 1) (Arz et al., 1998; Behling et al., 2002; Campos et al., 2019; Mulitza et al., 2017; Nace et al., 2014; Venancio et al., 2018). Runoff also does not track the western Amazon $\delta^{18}O$ records such that no single $\delta^{18}O$ record corresponds with basin-wide runoff trends. The discrepancy between records of continental runoff and interpretations of existing $\delta^{18}O$ data warrants revisiting the speleothem oxygen isotope data which remain in conflict (Cruz et al., 2009; Cheng et al., 2013; Wang et al., 2017).

Climate model simulations are often more consistent with SAPD-like precipitation anomalies, but not necessarily their isotopic expression. For example, models have found that increased northern hemisphere summer insolation in the mid-Holocene weakens the South American Monsoon, causing compensating changes in atmospheric circulation that decrease western Amazon rainfall and increase rainfall in the eastern Amazon and northeastern Brazil (Cruz et al., 2009; Liu & Battisti, 2015). However, the western decrease and eastern increase in rainfall is comparable, not imbalanced as predicted from the speleothem $\delta^{18}O$ data (Cruz et al., 2009; Liu & Battisti, 2015; Shimizu et al., 2020). Further, some models do not simulate SAPD behavior (Shimizu et al., 2020) and a closer inspection of the speleothem $\delta^{18}O$ data reveals that the trends are out-of-phase, with the highest western $\delta^{18}O$ occurring before the minima in the records further east (Fig. 1c-e). These asynchronous $\delta^{18}O$ trends challenge the prevailing SAPD model where precipitation changes are driven by the same atmospheric circulation anomaly (Cruz et al., 2009). We currently lack a conceptual model for the SAPD that is able to explain the zonally imbalanced $\delta^{18}O$ signals, their out-of-phase nature, and the apparent discrepancy with continental runoff data.

Here, we test whether a revised interpretation of the speleothem $\delta^{18}O$ data leads to better agreement with proxies, and we present new model analyses to test whether the strength of monsoon convection and its related compensating circulation (henceforth, monsoon strength) is the most likely driver of the late Quaternary SAPD. Our revised $\delta^{18}O$ interpretation uses spatial oxygen isotope gradients ($\Delta\delta^{18}O$; ‰/1000 km) to account for the degree of upwind rainout from an airmass—a factor that was not empirically constrained in previous $\delta^{18}O$ interpretations of the SAPD (van Breukelen et al., 2008; Cruz et al., 2009; Cheng et al., 2013; Wang et al., 2017). The degree of upwind rainout (where upwind is east) is widely known to drive Amazon $\delta^{18}O$ in modeling, observational, and paleoclimate studies (Salati et al., 1979; Grootes et al., 1989; Gat & Matsui, 1991; Vuille et al., 2003; Vimeux et al., 2005; Vuille & Werner, 2005; Brienen et al., 2012; J. C. A. Baker et al., 2016; Ampuero et al., 2020), potentially decoupling $\delta^{18}O$ from local precipitation amount (to which speleothem $\delta^{18}O$ trends are commonly attributed) (van Breukelen et al., 2008; Cruz et al., 2009; Cheng et al., 2013; Wang et al., 2017). Speleothem strontium isotope records provide evidence for $\delta^{18}O$ decoupling from rainfall amount at the eastern Amazon site (Ward et al., 2019) and across tropical South America more broadly (Wortham et al., 2017; Ward et al., 2019), emphasizing the limitations of interpreting $\delta^{18}O$ as a precipitation amount proxy in this region. We ultimately find that accounting for upwind rainout brings the speleothem $\delta^{18}O$ data in agreement with independent proxy records, including the strontium isotope data, and casts the SAPD as zonally balanced—with similar rainout in the western and eastern phases—despite zonally imbalanced $\delta^{18}O$ signals.

In the second part of our analysis, we present evidence for an alternative hypothesis to explain the zonally balanced SAPD and we test its plausibility for the late Quaternary. We hypothesize that the SAPD precipitation anomalies are driven by the east-west migration of the centroid of South American Monsoon rainout, such that the location of peak rainout changes while the amount of rainout does not. Previous work shows that the South American Monsoon (like the pan-Asian Monsoon; Battisti et al. (2014)) is energetically primed to migrate east-west (Boos & Korty, 2016). Such zonal shifts cause large changes in precipitation and $\delta^{18}O$ in the pan-Asian Monsoon region (Battisti et al., 2014), and we find similarly large changes in South American precipitation using an isotope-enabled reactive transport model. To test whether late Quaternary forcing could cause the South American Monsoon to migrate zonally, we impose plausible forcings in an energy balance model for monsoon circulation and find zonal shifts in the monsoon that support the proxy data. These forcings were not considered in previous climate model studies of the SAPD. We argue that the zonal monsoon migration hypothesis for the SAPD is consistent with key features of the $\delta^{18}O$ records, including their out-of-phase relationship. While monsoon migration can explain the SAPD precipitation anomalies over the last ∼25 kyr, we stress that the SAPD is an empirical rainfall pattern, not a dynamic mechanism, and different mechanisms than zonal monsoon migration may drive the SAPD anomalies in older records (Abouchami & Zabel, 2003; Mason et al., 2019).

2 Late Quaternary speleothem $\delta^{18}O$ records and monsoon dynamics

Our analysis leverages three existing speleothem $\delta^{18}O$ records that span tropical South America and have previously been used to identify the SAPD. We refer to these as the eastern, central, and western records (Fig. 1). The eastern record is from the Rio Grande do Norte site of northeastern Brazil and shows a 5-7‰ decrease in $\delta^{18}O$ from the LGM to early-mid Holocene interpreted as evidence for a weaker South American Monsoon (Cruz et al., 2009) (Fig. 1c). The central record comes from the Paraíso site in east-central Amazonia (Wang et al., 2017) and resembles the eastern record, but the $\delta^{18}O$ decrease lags behind by 1-2 kyr (Fig. 1d). Given its location near the monsoon's deep convective region, these data are considered evidence for stronger monsoon convection in the mid-Holocene, in conflict with the eastern record interpretation (Wang et al., 2017). The western record is a composite of the Diamante (Cheng et al., 2013) and Tigre Perdido (van Breukelen et al., 2008) records (Fig. 1e). We adopt the cave temperature correction for these records following Wang et al. (2017) (see also Ampuero et al. (2020); Kukla et al. (2021)), increasing $\delta^{18}O$ by 1.4‰ to account for its relatively cooler cave temperatures. These records are interpreted to reflect Amazon or western Amazon rainfall amount, with a muted $\delta^{18}O$ increase of ∼2.5‰ from the LGM to early Holocene indicative of drying, then a gradual decrease to wetter, present conditions that starts when the eastern and then central $\delta^{18}O$ records initially decrease. The western record stands out from the central and eastern records in that $\delta^{18}O$ increases, rather than decreases, from the LGM to the early-mid Holocene. This contrast defines the $\delta^{18}O$ expression of the SAPD, with the western phase at the LGM and eastern phase at the mid-Holocene representing end-member SAPD states (Cruz et al., 2009; Cheng et al., 2013).

Existing hypotheses of the underlying SAPD dynamics rely on isotope-enabled climate model experiments that test the effect of high northern-hemisphere summer insolation (either the mid-Holocene orbital configuration (Cruz et al., 2009) or even higher-

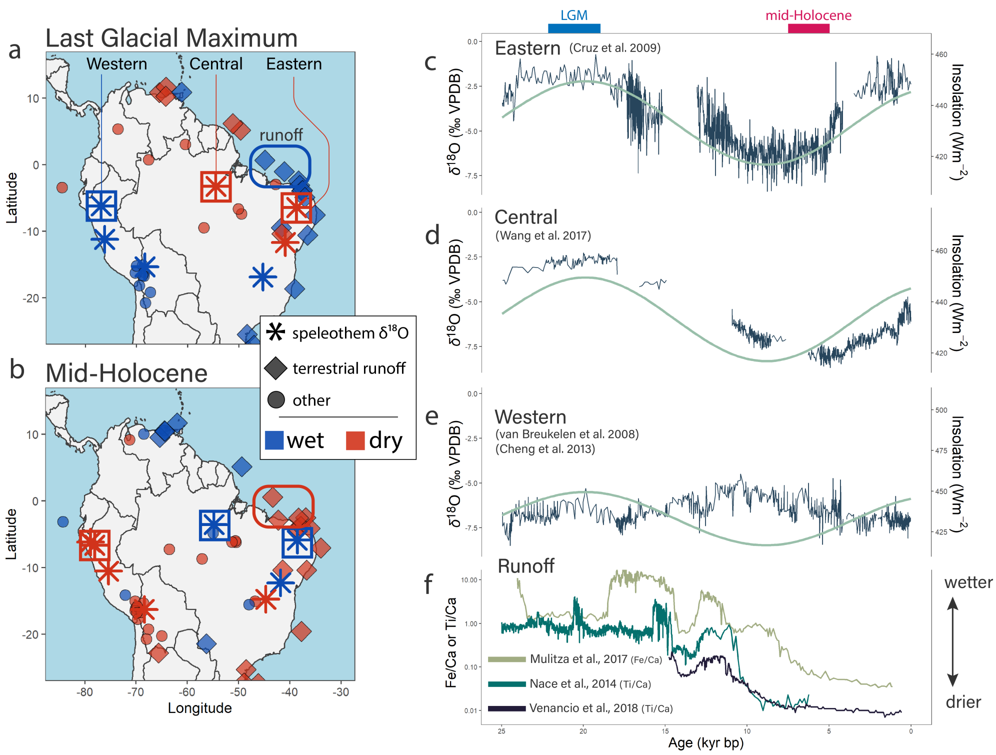

Figure 1. South America proxy map and isotope data. Proxy map for the LGM (~21 ka) (**A**) and mid-Holocene (~7 ka) (**B**). Data points in **A** and **B** are jittered to show instances of multiple proxy records from the same site. (**C**) Rio Grande do Norte (eastern) $\delta^{18}O$ record (Cruz et al., 2009). (**D**) Paraíso (central) $\delta^{18}O$ record (Wang et al., 2017). (**E**) Diamante and Tigre Perdido composite (western) $\delta^{18}O$ record (van Breukelen et al., 2008; Cheng et al., 2013). Teal lines (**C-E**) show February insolation at 10°S following Cruz et al. (2009) (scales varied to match $\delta^{18}O$ magnitude). **(F)** Runoff proxy data from Nace et al. (2014); Mulitza et al. (2017) and Venancio et al. (2018) with higher values indicating more runoff. Note the log scale in (F).

insolation (Liu & Battisti, 2015)). These studies show that high northern hemisphere summer insolation decreases the strength of the South American Monsoon and increases rainfall in northeast Brazil, although the mechanism for wetter conditions in the northeast is debated. Cruz et al. (2009) find that reduced moisture convergence in the South American Monsoon is balanced by reduced subsidence in northeast Brazil (see also Shimizu et al. (2020)), whereas Liu and Battisti (2015) find that cooling of South Africa leads to a north-shift and strengthening of the South Atlantic Convergence Zone. However, these studies did not simulate LGM conditions so the implications for the opposing, western SAPD phase at the LGM are unclear.

Each model is generally successful in reproducing the decrease in eastern $\delta^{18}O$ and increase in western $\delta^{18}O$ at the mid-Holocene relative to today, yet some key discrepancies remain. Both models under-predict the magnitude of $\delta^{18}O$ decrease at the eastern site, over-predict the magnitude of $\delta^{18}O$ increase at the western site, and find little-to-no $\delta^{18}O$ change over the central site (note that the central record was published after Cruz et al. (2009) and Liu and Battisti (2015)). One key limitation in the application of these models to the mid-Holocene is they do not account for the greening-induced decrease in Saharan land albedo—a major boundary condition change that has previously been linked to rainfall anomalies in tropical South America (Lu et al., 2021). If such zonal forcings can impact monsoon rainfall, they may be critical for explaining the zonal patterns of the SAPD.

Recent theoretical work demonstrates that the South American Monsoon, moreso than most other monsoon systems, is energetically primed to shift east-west due to changes in the zonal energy budget that could occur due to factors like non-local land surface albedo change (Boos & Korty, 2016). The South American Monsoon system sits at the intersection of the energy flux equator (correlated with the Inter-Tropical Convergence Zone; ITCZ) and an energy flux prime meridian (Boos & Korty, 2016). These energy flux lines occur where column-integrated divergent atmospheric energy transport is zero in the meridional (energy flux equator) and zonal (energy flux prime meridian) directions and their intersection approximates the rainfall maximum, or precipitation centroid, of the monsoon (Boos & Korty, 2016). This energy flux equator-prime meridian intersection conditions the South American Monsoon to migrate zonally because, just as the energy flux equator (and ITCZ) move north and south following anomalous meridional energy sources (*e.g.* changes in insolation and albedo), the energy flux prime meridian moves west and east in response to zonal energy anomalies. Previous work found that the pan-Asian Monsoon (the other monsoon system to exist at an energy flux line intersection) also shifts zonally due to asymmetric zonal forcing (Battisti et al., 2014). If the energy flux prime meridian shifted zonally in the past, we expect the monsoon centroid to shift with it (Boos & Korty, 2016), perhaps driving a zonal dipole in rainout expressed as the SAPD.

3 Methods

3.1 Paleo-isotope gradient justification

Isotope gradients measure the change in $\delta^{18}O$ ($\Delta\delta^{18}O$) between two sites that fall along a given moisture trajectory. This change in $\delta^{18}O$ is a metric for the net rainout of moisture from an air-mass between two sites and, in this way, is related to Rayleigh distillation interpretations of isotopic data ($\delta^{18}O$ and $\Delta\delta^{18}O$ decrease as distillation (rainout) increases) (Salati et al., 1979; Gat & Matsui, 1991). Whereas one must assume the upwind $\delta^{18}O$ value to interpret a given $\delta^{18}O$ record in terms of net rainout, $\Delta\delta^{18}O$ explicitly accounts for these upwind variations, theoretically isolating the $\delta^{18}O$ signal due to rainout alone (Hu et al., 2008; Winnick et al., 2014; Kukla et al., 2019, 2021). This approach is particularly useful in tropical South America because upwind effects are known to be a primary driver of $\delta^{18}O$ such that changes in $\delta^{18}O$ through time are likely to reflect a combination of changes in local versus upwind rainout (Salati et al., 1979; Gat & Matsui, 1991; Vuille et al., 2003; Vuille & Werner, 2005; Lee et al., 2009; Liu & Battisti, 2015; Ampuero et al., 2020). Upwind and local rainout can be distinguished because upwind rainout will change the initial $\delta^{18}O$ of a given domain but not $\Delta\delta^{18}O$ (Salati et al., 1979; Kukla et al., 2021). We note that $\Delta\delta^{18}O$ values are generally restricted to below zero (the "hydrostat"), since a zero isotope gradient reflects all precipitation being recycled between two sites or zero or negligible precipitation (i.e. no net rainout) (Caves et al., 2015; Chamberlain et al., 2014; Kukla et al., 2019).

To validate our use of the isotope gradient approach, we analyze the connectivity of moisture recycling among the eastern, central, and western sites in the modern climate using the 2-layer Water Accounting Model (WAM-2layers) (van der Ent et al., 2014) and the precipitation back-tracking scheme of Keys et al. (2012). We find that moisture recycling between our sites surpasses the threshold commonly used for identifying meaningful dynamical connections (Keys et al., 2012), demonstrating that these sites are sufficiently isotopically connected for $\Delta\delta^{18}O$ analysis (see Supplemental Text S1; Fig. S3). We also find that the modern isotope gradient across tropical South America is negatively correlated with rainout and is negative throughout the year, consistent with theory (Fig. S2).

3.2 Reconstructing paleo-precipitation rates from the central-to-western sites

We focus exclusively on the isotope gradient between the central and western sites for our quantitative precipitation reconstruction because this trajectory aligns best with that of prevailing monsoon winds (see Supplemental Text S1, S2). Oxygen isotope gradients along a dominant moisture trajectory depend on the balance of three fluxes: precipitation, evapotranspiration, and atmospheric transport (Salati et al., 1979; Winnick et al., 2014). We use a reactive transport model that simulates $\Delta\delta^{18}O$ as a function of these fluxes to quantify past precipitation rates from $\Delta\delta^{18}O$ data. To do so, we randomly sample from uniform distributions of reactive transport model input parameters to estimate past precipitation from the simulations that agree with $\Delta\delta^{18}O$ data (Kukla et al., 2019, 2021).

Our application of the reactive transport model to the central-to-western isotope gradient follows that of Kukla et al. (2021) with one key change. Kukla et al. (2021) used modern reanalysis data to analyze both the late Holocene and mid-Holocene isotope gradients because PMIP3/CMIP5 results show that reactive transport model inputs are similar for both time periods. However, modern reanalysis data cannot be reasonably applied to the LGM due to the ∼5°C of tropical cooling. To account for this cooling, we apply temperature-based scaling relationships to the reanalysis data to estimate LGM moisture content over the ocean (moisture source region) and potential evapotranspiration. Source region moisture content is calculated assuming relative humidity remains constant over the ocean, as predicted with future climate change (Sherwood et al., 2010), and potential evapotranspiration is decreased following the scaling relationship defined by Scheff and Frierson (2014) and Siler et al. (2019). Moisture content and humidity are allowed to change over land depending on model-simulated rainout. We further account for unique LGM conditions by restricting the wind speed and transpiration fraction estimates. Proxy studies (McIntyre & Molfino, 1996; Bradtmiller et al., 2016; Venancio et al., 2018) suggest that the northeasterlies were stronger at the LGM, so we restrict wind speeds to be equal to or greater than the late Holocene. Lower atmospheric pCO_2 implies lower plant water use efficiency suggesting that more transpiration may have been necessary to fix (approximately) the same amount of carbon. Since the rainforest largely remained intact at the LGM (*i.e.* similar biomass), we assume the transpired fraction of evapotranspiration is also equal to or greater than modern.

We find that our results are not sensitive to the shape of the distributions of model inputs, nor the sample size of the Monte Carlo routine (Fig. S4). We also test the importance of an additional input, rain re-evaporation, on model $\delta^{18}O$. Rain re-evaporation and its effect on $\delta^{18}O$ is heavily parameterized in models because it is difficult to directly measure (Worden et al., 2007; Dee et al., 2015; Konecky et al., 2019) (see Supplementary text S2-S3). Using a parameterization fit to isotope data we find that it has a negligible effect on $\delta^{18}O$ in the model (Fig. S5). Diagnostics of our late Holocene Monte Carlo results (essentially a modern analysis because speleothem $\Delta\delta^{18}O$ is the same as modern rainfall) are provided in Fig. S6.

We further use the reactive transport model to calculate spatial $\delta^{18}O$ patterns for individual PMIP3/CMIP5 models. Using zonal profiles of atmospheric moisture content, zonal winds, potential evapotranspiration, and temperature from the individual PMIP3/CMIP5 models, we run the reactive transport model to simulate the isotope gradient for the LGM, mid-Holocene, and late Holocene (PMIP3/CMIP5 pre-industrial). We then compare the predicted $\Delta\delta^{18}O$ derived from the PMIP3/CMIP5 data to the speleothem data. If the predicted $\Delta\delta^{18}O$ is more negative than the observed $\Delta\delta^{18}O$, then the net rainout in that model is too high to reconcile the observed data in the reactive transport frameowork. We further analyze the precipitation rate necessary to match the paleo-isotope gradient if all other PMIP3/CMIP5 inputs to the reactive transport model are correct. This analysis effectively asks how much rainfall must increase or decrease relative to the PMIP3/CMIP5 prediction in order to reconcile the paleoclimate $\Delta\delta^{18}O$ data.

3.3 Application of a 2-dimensional monsoon energy balance model

We use a 2-dimensional monsoon energy balance model that is capable of tracking zonal monsoon shifts (Boos & Korty, 2016) to accomplish two related goals. First, we use the energy balance model and reactive transport model to test whether the PMIP3/CMIP5 models show zonal monsoon shifts and are consistent with speleothem $\Delta\delta^{18}O$ data. Second, we analyze monsoon behavior under conditions that likely characterize the LGM and mid-Holocene but are not accounted for in the PMIP3/CMIP5 experiments.

The energy balance model predicts how changes in energy input to the atmosphere would change atmospheric energy transport, thus altering atmospheric circulation and precipitation patterns. Here, we follow the methodology of Boos and Korty (2016) and consider how changes in continental albedo alter energy input to the atmosphere, and how atmospheric circulation would have to adjust in order to maintain the energy balance. The anomalous energy flux generated by the energy balance model is then used to infer a shift in precipitation based on the assumption that the position of peak precipitation migrates with the intersection of the energy flux equator and energy flux prime meridian (see equations 2-7 in Boos and Korty (2016)).

3.3.1 Analysis of PMIP3/CMIP5 monsoon dynamics

Using the energy balance model, we identify the PMIP3/CMIP5 ensemble mean location of the monsoon precipitation centroid, defined as the intersection of the energy flux equator and prime meridian, for the LGM, mid-Holocene, and pre-industrial (or late Holocene). The LGM and mid-Holocene ensemble means are then used as the initial conditions for the perturbations discussed in the next section.

3.3.2 Simulating additional LGM and mid-Holocene constraints

A critical step in determining whether the South American Monsoon migrated zonally in the past is quantifying the sensitivity of zonal shifts to energetic forcing. We impose anomalous moist static energy sources in the PMIP3/CMIP5 ensemble mean to quantify how the zonal location of the energy flux prime meridian (and thus monsoon rainfall centroid (Boos & Korty, 2016)) changes with zonal forcing. The response of the South American Monsoon rainfall centroid to anomalous energy forcing depends on (*1*) the magnitude and direction of energetic forcing; (*2*) the area over which the forcing is applied; and (*3*) the distance (especially zonally) of the anomalous forcing to the monsoon.

During the mid-Holocene, lower land surface albedo likely increased the net column energy over the grassy "green" Sahara by about 70 W/m^2, accounting for the attuenuation of the albedo anomaly at the top of the atmosphere (Boos & Korty, 2016). This forcing exceeds the magnitude of insolation change due to orbital variability (∼10 W/m^2 in the mid-Holocene), but is applied over a smaller area (confined to the modern Sahara). Other modeling investigations of the late Quaternary SAPD (including PMIP3/CMIP5 simulations) accounted for orbital forcing, but did not consider the Green Sahara (Cruz et al., 2009; Liu & Battisti, 2015). During the LGM there is evidence for forest dieback and grassland expansion in the African tropics, plus tundra expansion in the forests of modern Eurasia (Wu et al., 2007; Prentice et al., 2011; Binney et al., 2017). These vegetation shifts would have brightened the regional land surface and, barring strong compensating feedbacks, the top of atmosphere. We note that our analysis does not account for other factors outside of moist static energy anomalies that can shift the precipitation centroid zonally. For example, there is evidence for stronger easterly winds across the tropical Atlantic at the LGM (McIntyre & Molfino, 1996; Adkins et al., 2006; McGee et al., 2013; Bradtmiller et al., 2016; Zular et al., 2019) that could shift the maximum vector wind divergence, and thus monsoon centroid, westward, but stronger winds cannot be readily integrated to the energy balance model as an anomalous energy source.

Starting from the ensemble mean mid-Holocene and LGM climates, we simulate the effect of a darker Sahara (mid-Holocene) and a brighter African tropics and Eurasia (LGM) as spatially uniform positive and negative moist static energy anomalies, respectively. This approach carries some important limitations and should be taken as a proof of concept for demonstrating how land surface albedo can modulate the zonal location of the South American Monsoon precipitation centroid. Our analysis implicitly assumes that the attenuation of the land surface anomaly to the top of atmosphere is spatially uniform, which is unlikely when comparing tropical Africa and Eurasia. This analysis also ignores the role of an apparent shift to a less El Niño-dominant mean climate state after the LGM (Koutavas & Joanides, 2012; Ford et al., 2018). The El Niño Southern Oscillation impacts Amazon rainfall (Marengo et al., 2013) and is a primary mode of zonal energy anomalies in the modern climate (Boos & Korty, 2016), but its behavior is uncertain in paleoclimate models (Zheng et al., 2008; Brierley & Wainer, 2018). To our knowledge, El Niño dynamics have not been explicitly considered as drivers of the late Quaternary SAPD in previous work.

4 Results and interpretation

4.1 Isotope gradients and net rainout

The isotope gradients over space are distinct from any one $\delta^{18}O$ record, suggesting there is no single representative site that reflects basin-wide rainout. Figure 2a shows these gradients for the eastern-to-central sites ("eastern domain"; light green) and central-to-western sites ("western domain"; dark green), with the theoretical maximum $\Delta\delta^{18}O$ value of zero labelled as the hydrostat (Chamberlain et al., 2014; Caves et al., 2015; Kukla et al., 2019). The eastern domain gradient is near the hydrostat from the LGM to the early Holocene, then decreases to ∼-2.5‰ in the mid-late Holocene and increases by <1‰ to present. The western domain gradient shows a mostly opposing trend, with $\Delta\delta^{18}O$ near ∼-2‰ at the LGM and increasing to zero, the hydrostat, by the mid-Holocene before decreasing to present. The late Holocene $\Delta\delta^{18}O$ value in this domain is similar to the rainfall $\Delta\delta^{18}O$ across the Amazon today (Salati et al., 1979; Wang et al., 2017). Overall, despite $\delta^{18}O$ shifts that are zonally imbalanced (about twice as large in the eastern

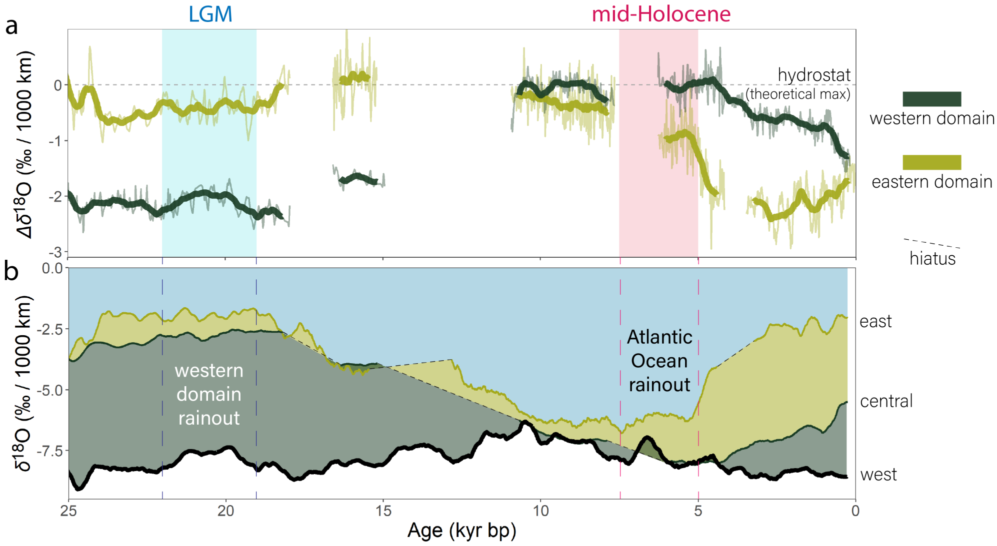

Figure 2. Isotope gradient and individual $\delta^{18}O$ records. (**A**) Eastern-to-central (light green) and central-to-western (dark green) isotopic gradients. More negative $\Delta\delta^{18}O$ is interpreted as more rainout between sites (wetter). (**B**) The three, smoothed $\delta^{18}O$ records (labels on right of panel). Y-axis color range is proportional to net moisture loss (rainout) within the western (dark green), eastern (light green), or ocean (turquoise) domains. The increase in blue toward the MH reflects a hypothesized increase in rainout over the ocean. Dashed lines with intervals of lighter shading are hiatus periods in the $\delta^{18}O$ records.

and central records compared to the west), the magnitude of $\Delta\delta^{18}O$ change is comparable in each domain, consistent with zonally balanced changes in rainout.

Following previous work using isotope gradients (Salati et al., 1979; Hu et al., 2008; Winnick et al., 2014), we interpret the $\Delta\delta^{18}O$ data as reflecting rainout between two sites and the $\delta^{18}O$ data as recording the net integrated upwind rainout signal. Figure 2b is an attempt to visualize both the local ($\Delta\delta^{18}O$) and upwind ($\delta^{18}O$) rainout signals. Here, the eastern, central, and western $\delta^{18}O$ records are smoothed and plotted together with the space between them colored to illustrate the magnitude of change in $\delta^{18}O$ between each site. This figure shows that the location where $\delta^{18}O$ decreases the most (indicative of the most rainout) shifts from the western domain (dark green) at the LGM to east of the eastern site, over the tropical Atlantic Ocean (blue), by the mid-Holocene.

This interpretive framework explains how the SAPD is zonally balanced despite zonally imbalanced $\delta^{18}O$ records. The western $\delta^{18}O$ shifts are small compared to the eastern record because the focus of rainout is always upwind of the western site. In contrast, the focus of rainout is downwind of the eastern and central sites at the LGM, and upwind of these sites at the mid-Holocene. Put otherwise, the focus of rainout shifts along the moisture trajectory relative to the eastern and central sites, but not the western site, driving larger amplitude $\delta^{18}O$ trends in the eastern and central sites.

In addition to the zonally imbalanced $\delta^{18}O$ trends, another enigmatic feature of the $\delta^{18}O$ data is that the records are out-of-phase with one another. The out-of-phase nature of these $\delta^{18}O$ shifts can also be understood in the context of upwind effects. The western $\delta^{18}O$ record decreases from 10-5 ka (Fig. 2b) while $\Delta\delta^{18}O$ stays near the theoretical maximum value of zero (Fig. 2a), consistent with the $\delta^{18}O$ shift being driven by upwind rather than local rainout. Meanwhile, in the last 5 kyr, the focus of decreas-

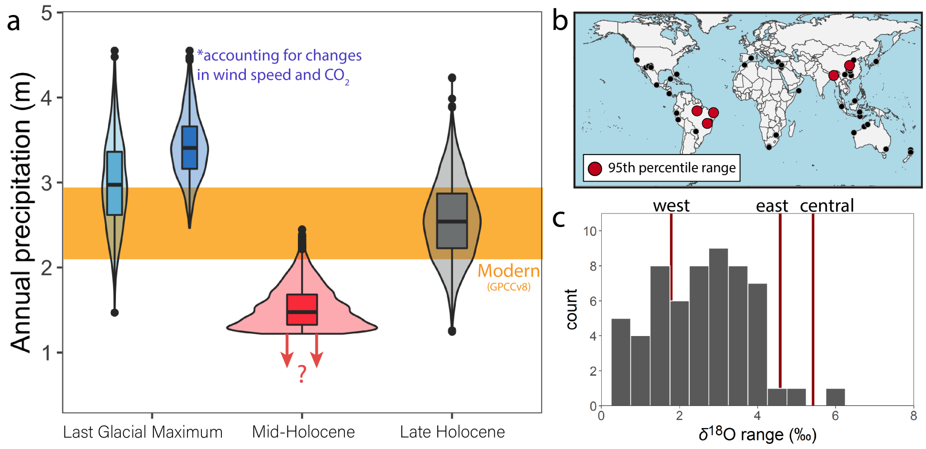

Figure 3. (**A**) Reconstructed precipitation for the LGM (blue), mid-Holocene (red) and late Holocene (gray). Mid-Holocene is restricted at the lower-bound because $\Delta\delta^{18}O$ is at the hydrostat. (**B-C**) Map of $\delta^{18}O$ records with $\delta^{18}O$ ranges in the largest 5% (red) and all sites (black) and the distribution of $\delta^{18}O$ ranges. The central and eastern records are in the largest 5 percent of all similar sites (Supplemental text S4).

ing $\delta^{18}O$ shifts inland, first over the eastern domain and next over the western domain, revealing a time-transgressive trend that emerges from the central $\delta^{18}O$ data lagging the eastern record. Thus, the progressive inland migration of the focus of rainout provides a plausible mechanism for the enigmatic lag between these records.

4.2 Reconstructed annual precipitation rates

Our reactive transport results suggest that late Holocene precipitation rates were similar to modern, consistent with similar $\Delta\delta^{18}O$ values between the late Holocene speleothem data and modern rainfall. During the LGM, we find increased rainfall relative to the late Holocene (light blue distribution of Fig. 3a; 3000 $\pm$ 800 mm/yr). This result is consistent with independent proxy data pointing to more continental runoff (Mulitza et al., 2017; Nace et al., 2014; Venancio et al., 2018) and wetter conditions in western tropical South America (P. A. Baker, Seltzer, et al., 2001; P. A. Baker, Rigsby, et al., 2001; Fritz et al., 2004). When wind speed and transpiration are equal to or greater than modern values (see Methods), calculated rainfall increases to $\sim$3400 $\pm$400 mm/yr to compensate for increased moisture transport and decreased isotopic fractionation associated with transpiration (dark blue distributions of Fig. 3a). We note that hydrogen isotope composition (δD) of leaf waxes from the Amazon River appears higher at the LGM than before or after, suggesting drier conditions than today (Häggi et al., 2017). We suggest this trend could be driven by an increased eastern Amazon (higher-δD) vegetation input to the Amazon River. Häggi et al. (2017) note that this effect is unlikely due to higher precipitation in the west, but we suggest a greater input of eastern biomass could occur due to destabilization of vegetation in the east during drier, colder conditions.

During the mid-Holocene, the reactive transport model simulates rainfall decreasing to $\sim$1200 mm/yr (about half of modern; red distribution of Fig. 3a). As discussed in Kukla et al. (2021), the $\Delta\delta^{18}O$ values in the mid-Holocene straddle zero—the theoretical maximum value for a single moisture trajectory. At this point, further drying has a negligible effect on $\Delta\delta^{18}O$. The shape of the mid-Holocene distribution thus reflects the imposed lower-bound of annual precipitation, effectively restricting the solution to the wettest scenarios.

One limitation to our analysis is that we do not explicitly account for the possibility that changes in the seasonality of rainfall affect one site more than the other. Such changes can modify the spatial gradient in $\Delta\delta^{18}O$ without changing net rainout. The reconstructed isotope gradient in the western domain, however, provides some support that seasonal biases in precipitation do not overprint the $\Delta\delta^{18}O$ data (Fig. S7). If localized shifts in seasonality drove the $\delta^{18}O$ data we would expect to find $\Delta\delta^{18}O$ values greater than zero due to seasonal overprinting, especially when isotope gradient is already shallow (near-zero $\Delta\delta^{18}O$). Instead, we find that when the isotope gradient becomes shallow, the upwind and downwind $\delta^{18}O$ records shift in tandem (leading to changes in $\delta^{18}O$ but no change in $\Delta\delta^{18}O$), suggesting upwind signals fully propagate inland without seasonal overprinting (*i.e.* a high degree of isotopic connectivity).

The estimates of past precipitation form the reactive transport model show larger precipitation anomalies than predicted by the Earth System Models used to link the SAPD to monsoon strength (Cruz et al., 2009; Liu & Battisti, 2015; Shimizu et al., 2020). Thus, if the speleothem $\delta^{18}O$ data reliably reflects past precipitation, we must consider the possibility that monsoon strength is not the primary driver of the late Quaternary SAPD. Changes in the location of monsoon rainout are likely to have a greater effect on local (east vs west) annual rainfall amounts than changes in the strength of monsoon rainout. For example, Battisti et al. (2014) argues that a zonal shift in the pan-Asian monsoon with changing northern hemisphere summer insolation could explain some of the largest documented speleothem $\delta^{18}O$ shifts. Using the SISALv2 database (Atsawawaranunt et al., 2018; Comas-Bru et al., 2019, 2020) we find that magnitude of $\delta^{18}O$ shifts in the eastern and central records is in the top 5% of all comparable records (duration between 10^3–10^5 years and within 40° of the equator) (see Supplemental text S4) (Fig. 3b, c). The other records with large $\delta^{18}O$ ranges appear near the pan-Asian monsoon region, consistent with these two monsoon systems being among the most sensitive to zonal energy anomalies and monsoon migration (Battisti et al., 2014; Boos & Korty, 2016).

4.3 PMIP3/CMIP5 analysis with energy balance and reactive transport models

Our analyses with the PMIP3/CMIP5 data affirm previous isotope-enabled Earth System Model results (Cruz et al., 2009; Liu & Battisti, 2015). The simulations do not capture zonal migration of the monsoon centroid and they under-estimate the magnitude of $\delta^{18}O$ variation (Battisti et al., 2014). We find that, while the energy flux equator shifts northward in the mid-Holocene, the energy flux prime meridian does not show any systematic shift to the east or west (Fig. 4a). Meanwhile, when forced with PMIP3/CMIP5 output the reactive transport model correctly predicts late Holocene $\Delta\delta^{18}O$ data, demonstrating that the net rainout in the models is consistent with the isotope data. During the LGM, however, the PMIP3/CMIP5 output leads to an isotope gradient that is too shallow, consistent with the models being too dry (Fig. 4b,c). In contrast, the simulated isotope gradients are too steep at the mid-Holocene when driven by PMIP3/CMIP5 output, consistent with the models being too wet. Taken together, zonal monsoon shifts are negligible in the PMIP3/CMIP5 models and their precipitation anomalies are smaller than suggested by the isotope data.

We therefore hypothesize that the zonal migration of the South American Monsoon precipitation centroid drives the late Quaternary SAPD and its isotopic expression. This hypothesis is outlined in Figure 5, and we address its plausibility in the following subsection. We hypothesize that the monsoon centroid existed between the central and western records at the Last Glacial Maximum (Fig. 5c, f), upwind of the eastern record at the mid-Holocene (Fig. 5b, e), and somewhere in between in the late Holocene (Fig. 5a, d), consistent with its modern position (Boos & Korty, 2016). This evolution of the monsoon centroid is based on the region where the decrease in $\delta^{18}O$ is greatest (indicative of the most rainout) or upwind of the three records when the eastern $\delta^{18}O$ values

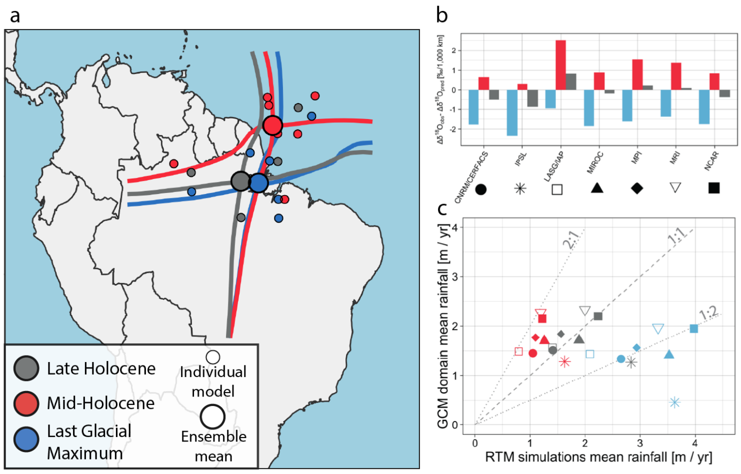

Figure 4. PMIP3/CMIP5 SAM centroid and isotope gradient analysis. (**A**) PMIP3 models show little zonal variation in the South American Monsoon precipitation centroid from the LGM, mid-Holocene, and late Holocene (pre-industrial) for months NDJFMAM. (**B**) When forced with PMIP3/CMIP5 output, the reactive transport model (Kukla et al., 2019) systematically predicts a steeper-than-observed $\delta^{18}O$ gradient at the mid-Holocene (red bars) and a shallower-than-observed gradient at the LGM (blue bars) with no systematic error in the late Holocene. This result is consistent with the $\delta^{18}O$ error found in the isotope-enabled simulations of Cruz et al. (2009) and Liu and Battisti (2015). (**C**) To match the observed oxygen isotope gradient, the reactive transport model requires similar rainfall amounts as predicted by the PMIP3/CMIP5 models at the late Holocene, but requires drier conditions than PMIP3/CMIP5 at the mid-Holocene and wetter conditions at the LGM.

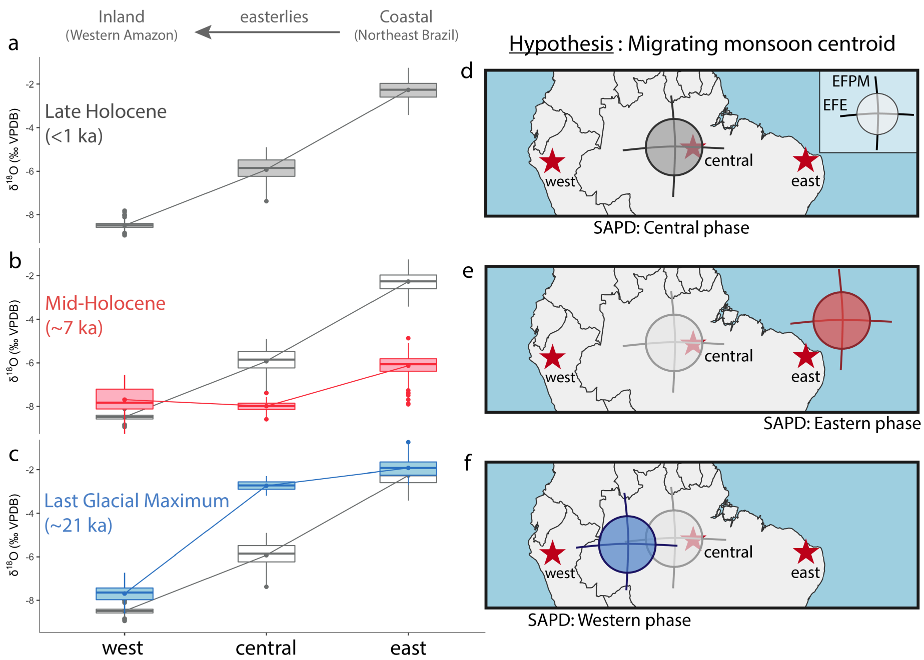

Figure 5. Monsoon migration hypothesis and its isotopic expression. (**A-C**) Show the three distinct isotope profiles of the late Holocene (**A**), mid-Holocene (**B**), and LGM (**C**). Late Holocene is reproduced in panels **B** and **C** for comparison. Lines connect the mean of each site. (**D-F**) Illustrate hypothesized changes in the South American Monsoon centroid (intersection of the energy flux equator (EFE) and energy flux prime meridian (EFPM)) based on where most of the $\delta^{18}O$ decrease (rainout) occurs (tropical Atlantic/northeast Brazil at mid-Holocene, and western Amazon at LGM).

are lowest. While zonal monsoon migration aligns with the $\delta^{18}O$ data and its magnitude of change, it is unclear whether late Quaternary forcings could plausibly drive such zonal shifts in the late Quaternary.

4.4 Zonal monsoon migration in an Energy Balance Model

We find that reasonable zonally asymmetric forcings for the mid-Holocene and LGM, not captured in the PMIP3/CMIP5 models, can cause the monsoon to shift zonally relative to its initial PMIP3/CMIP5 ensemble mean state (Fig. 6). In our energy balance model simulations, the anomalous moist static energy source owed to a darker Sahara at the mid-Holocene is sufficient to pull the energy flux prime meridian east of the eastern speleothem record, consistent with its mid-Holocene $\delta^{18}O$ minimum (Fig. 6d-f). In contrast, a decrease in forest cover in tropical Africa and Eurasia pushes the energy flux prime meridian westward in the LGM (Fig. 6a-c). We note that the location of the energy flux equator-prime meridian intersection approximates, but may be offset from, the location of the precipitation centroid (Boos & Korty, 2016). Nonetheless, the spatial shifts in the energy flux lines are highly correlated with spatial shifts in the precipitation field (Adam et al., 2016; Boos & Korty, 2016). Thus, this analysis emphasizes that the distance that the precipitation centroid migrates due to remote forcing is likely sufficient to explain the late Quaternary precipitation anomalies, although the exact location of monsoon rainout will depend on the initial state (here, from PMIP3/CMIP5) and the relative offset between the energy flux intersection and the precipitation centroid.

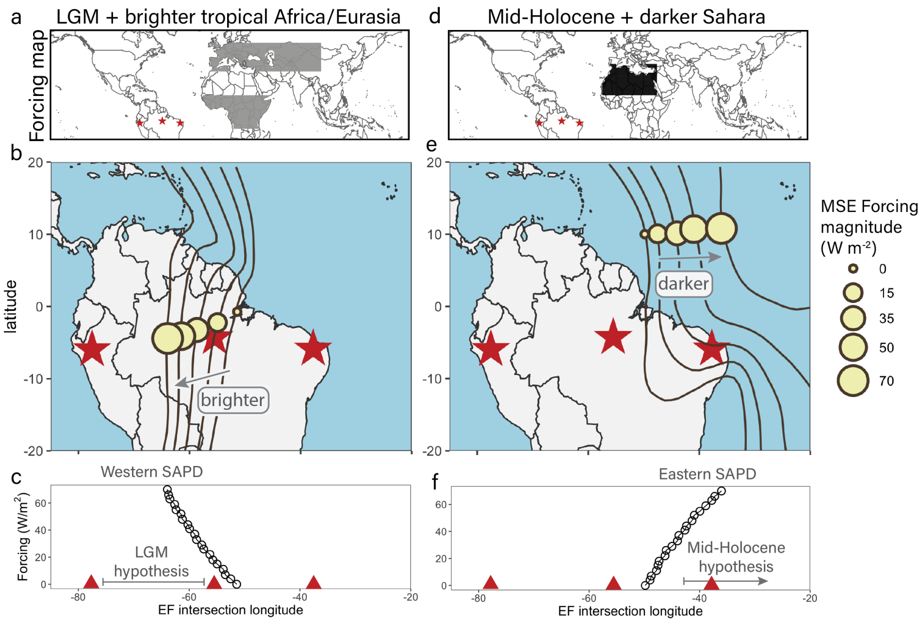

Figure 6. Sensitivity of the SAPD to zonal energy anomalies. Gray and black boxes in the maps of panels (**A**) and (**D**) show the locations of LGM and mid-Holocene moist static energy (MSE) forcings, respectively. Panels (**B**) and (**E**) show the response of the energy flux prime meridian (lines) and energy flux intersection (points; approximating the monsoon rainfall centroid) to selected forcing levels for the LGM and mid-Holocene. The energy flux intersection longitude versus the magnitude of forcing is shown in panels (**C**) and (**F**) for the LGM and mid-Holocene. We note that the points on the map panels are not a proposed path of the monsoon precipitation centroid in the Late Quaternary, but rather the monsoon response to different forcing magnitudes starting from the PMIP3/CMIP5 initial conditions.

5 Discussion

5.1 A zonally balanced SAPD

Previous work has argued that the distinct trends between the western and central/eastern $\delta^{18}O$ data reflect either (1) a zonally imbalanced precipitation dipole (Cruz et al., 2009; Cheng et al., 2013); or (2) changes in the strength of monsoon convection, but not the location of monsoon rainout (Wang et al., 2017). Here, we address how our results support a third scenario—a zonally balanced SAPD—and reconcile the $\delta^{18}O$ data with independent proxies. We also discuss how accounting for upwind rainout distinguishes our revised $\delta^{18}O$ interpretations from previous work.

The muted $\delta^{18}O$ shifts in the western record compared to the larger $\delta^{18}O$ shifts toward the east were previously cited as evidence that the SAPD disproportionately affects eastern Amazonia with dampened precipitation change in the west (Cheng et al., 2013). This is a reasonable result when interpreting $\delta^{18}O$ trends as reflecting local rainout. However, when accounting for upwind effects, downwind $\delta^{18}O$ should be minimally affected by changes in the *location* of upwind rainout. That is, whether the focus of rainout occurs near the speleothem site or a few hundred kilometers upwind, speleothem $\delta^{18}O$ will be approximately the same so long as the same magnitude of rainout occurs before the airmass reaches that site. We argue that this is why the western $\delta^{18}O$ trends are muted—the focus of rainout remains upwind of the western site for the entirety of the record. In contrast, the focus of rainout moves from downwind (inland) of the central and eastern sites at the LGM to upwind (coastal) of these sites at the mid-Holocene. In this way, the magnitude of total rainout is relatively constant (as evidenced by the muted western $\delta^{18}O$ record), regardless of whether that rainout occurs in the west or east. In other words, the western and eastern legs of the SAPD are balanced.

Using the same $\delta^{18}O$ data as our study, but a different interpretive framework, previous work argued that the central $\delta^{18}O$ record reflects the strength of South American Monsoon convection without invoking a zonal precipitation dipole (Wang et al., 2017). Wang et al. (2017) assume that upwind $\delta^{18}O$ is constant (with corrections for temperature and seawater $\delta^{18}O$) such that the central $\delta^{18}O$ record drives all variability in $\Delta\delta^{18}O$, and they find a wet mid-Holocene (~3400 mm/yr) and drier LGM (~1400 mm/yr). However, this assumption of an effectively constant upwind $\delta^{18}O$ value is refuted by data (Cruz et al., 2009)—the strong correlation between central and eastern (upwind) $\delta^{18}O$ records is evidence that upwind $\delta^{18}O$ is influencing the downwind signal, especially given that upwind signals from the eastern site should propagate to the central site today (Supplementary Text S1). Our approach avoids the assumption that upwind moisture loss is constant through time and, as a result, we find that the wettest time occurs when the isotope gradient is steepest, not when central $\delta^{18}O$ is lowest. Previous work argues that a shallower isotope gradient at the mid-Holocene can be reconciled with wetter conditions if increased transpiration causes the isotope gradient to shallow (Cheng et al., 2013; Wang et al., 2017). However, this effect has been shown to be isotopically negligible or at least too small to explain the $\Delta\delta^{18}O$ data based on modeling and observational evidence (Pattnayak et al., 2019; Ampuero et al., 2020).

The primary limitation of these two previous $\delta^{18}O$ interpretations (Cheng et al., 2013; Wang et al., 2017) is that both imply that the increase in precipitation at the eastern and central sites toward the mid-Holocene must outpace drying in the west—a result that is difficult to reconcile with low mid-Holocene continental runoff (Campos et al., 2019; Mulitza et al., 2017; Nace et al., 2014; Venancio et al., 2018). By accounting for upwind rainout, we show that eastern and central $\delta^{18}O$ are low at the mid-Holocene mostly because of upwind rainout that did not occur over land, consistent with low runoff (Campos et al., 2019; Mulitza et al., 2017; Nace et al., 2014; Venancio et al., 2018).

Overall, the speleothem $\delta^{18}O$ data show that total continental rainout correlates with continental runoff for most of the last 25 kyr, and this result cannot be inferred from amount effect interpretations of speleothem $\delta^{18}O$ in South America alone. However, there remains a discrepancy between our revised isotope interpretation and the continental runoff proxy data in the last 3-5 kyr, as western domain $\Delta\delta^{18}O$ (central-to-western record) decreases while Amazon runoff does not appear to increase. Still, more local proxy data shows generally wetter conditions in east-central Amazonia in the last 5 kyr (Reis et al., 2017; Ward et al., 2019), suggesting wetting here may be balanced by drying elsewhere, counteracting any increase in runoff. We note that there is no such discrepancy between runoff and the eastern domain $\Delta\delta^{18}O$—runoff from northeastern Brazil increases in the last 5 kyr as $\Delta\delta^{18}O$ decreases (Arz et al., 1999; Behling et al., 2002; Gu et al., 2017; Campos et al., 2019; Jaeschke et al., 2007).

5.2 Monsoon strength versus monsoon migration

A zonally balanced SAPD can be explained by changes in the strength of the monsoon (with its compensating circulation) (Cruz et al., 2009; Liu & Battisti, 2015) and changes in its location (via zonal migration). As discussed earlier, a weaker monsoon has been found to decrease rainout in western Amazonia and increase it in northeastern Brazil via balancing overturning circulation (Cruz et al., 2009; Shimizu et al., 2020) or a remote response of the South Atlantic Convergence Zone to cooling over South Africa (Liu & Battisti, 2015). Meanwhile, the migration of the monsoon centroid from the western Amazon at the LGM to the northeast at the mid-Holocene would have the same effect—rainout decreases in the west and increases proportionately in the east.

We attempt to distinguish between monsoon strength and monsoon migration under the premise that monsoon migration will lead to higher-amplitude $\delta^{18}O$ and precipitation change (Battisti et al., 2014). Indeed, the central and eastern $\delta^{18}O$ shifts (the records most affected by monsoon migration) are are among the largest documented, similar to the pan-Asian Monsoon, and Earth System Models tend to predict smaller changes in $\delta^{18}O$ and precipitation compared to observations and $\delta^{18}O$-derived precipitation estimates (Cruz et al., 2009; Liu & Battisti, 2015; Shimizu et al., 2020; Wang et al., 2017). The apparent disagreement between Earth System Models and proxy-based estimates could indicate that more complex models are not simulating key processes driving precipitation $\delta^{18}O$. However, we cannot rule out the possibility that speleothem $\delta^{18}O$ does not accurately reflect precipitation $\delta^{18}O$. We note that previous work has found discrepancies between $\delta^{18}O$ and *local* rainout, suggesting that $\delta^{18}O$ is at least not always tracking local precipitation (Ward et al., 2019; Wortham et al., 2017). However, as discussed in the next section, these results are consistent with our interpretation of $\delta^{18}O$ as a proxy for upwind rainout. Taken together, without evidence against speleothem $\delta^{18}O$ as an upwind rainout signal, the large magnitude of central and eastern $\delta^{18}O$ shifts along with the modeled magnitude of precipitation change is inconsistent with monsoon strength as a driver for the SAPD.

5.3 Zonal and meridional components of monsoon migration

In addition to the magnitude of isotopic signals, monsoon migration may be distinguished from monsoon strength through the temporal and spatial characteristics of proxy records. For example, monsoon migration should lead to both zonal and meridional shifts in the South American Monsoon precipitation centroid. The energy flux equator drives north-south migration that is well-documented in late Quaternary proxy records (Arbuszewski et al., 2013; Deplazes et al., 2013), and the energy flux prime meridian drives the east-west component (Boos & Korty, 2016). Because the location of the South American Monsoon varies near-linearly with anomalous forcing (rather than abruptly at some threshold; Fig. 6) the spatial migration of the South American Monsoon should cause time-transgressive proxy trends as it reaches different locations at different times. Here, we compare the west-east (LGM to mid-Holocene) and east-west (mid-Holocene to present) SAPD transitions and discuss evidence for zonal and meridional structure of monsoon migration with asynchronous proxy signals, consistent with our hypothesis.

We first focus on a broad comparison of the two SAPD transitions by comparing the eastern-to-central (eastern domain) and central-to-western (western domain) $\Delta\delta^{18}O$ data, shown in Figure 7b. Here, lower values on the y-axis are interpreted as more western domain rainout, and lower values on the x-axis as more eastern domain rainout. If the focus of rainout only migrates zonally, then a west-east trade-off in rainout will mark a diagonal line with slope -1 (as rainout in one domain increases at the expense of the other), and a shift in rainout further east over the ocean will trace a flat line with an intercept near zero (no rainout in the western domain, only moving through the eastern domain) (Fig. 7c, "expected if only zonal"). The $\Delta\delta^{18}O$ data, however, do not follow this trend. Instead, the LGM to early-mid Holocene marks a decrease in western domain rainout (increase in y-axis) with no compensating increase in the east (x-axis remains near zero) (Fig. 7b, points 1-2), followed by a mostly zonal progression into the eastern, then western domain (points 2-3 and 3-4, respectively). The focus of monsoon rainout appears to migrate eastward with a meridional component relative to the speleothem sites from the LGM to early-mid Holocene, and then westward following a zonal pattern through the speleothem sites to present.

This inferred pattern of monsoon migration from the $\Delta\delta^{18}O$ data is supported by independent proxy results. In the last eight thousand years, for example, a steeper isotope gradient reflecting more moisture distillation first appears in the eastern domain from ∼8-5 ka (points 2-3 of Fig. 7), and next in the western domain from ∼5-0 ka (points 3-4) (see also Fig. 2). This result suggests that the precipitation centroid began passing over the central record ∼5 thousand years ago, consistent with recent strontium isotope evidence from the same site pointing to high infiltration rates from 6-5 ka with less infiltration before and after (Ward et al., 2019). The timing of migration is also consistent with a shift from dry to wet conditions in a nearby lake (Reis et al., 2017). After ∼5 ka, rainfall begins increasing in the western domain and water infiltration rates at the central site temporarily decline (Ward et al., 2019). As discussed earlier, this gradual westward migration of monsoon rainout also explains the perplexing lag of central $\delta^{18}O$ behind the eastern record (Fig. 1c, d). The precipitation centroid first reaches the eastern site at ∼8-7 ka when $\delta^{18}O$ values are lowest, and later the central site at ∼5 ka, in tandem with records of the local water balance (Reis et al., 2017; Ward et al., 2019).

Unlike this east-west migration, the dipole transition from west to east spanning ∼20-10 ka does not coincide with a decrease in eastern domain $\Delta\delta^{18}O$, and we suggest this reflects the precipitation centroid moving around, rather than through, the eastern domain (points 1-2 of Fig. 7). Movement around the domain would require a meridional component of monsoon migration reflected by a change in $\Delta\delta^{18}O$ in one domain that is not balanced by a corresponding change in the other (Fig. 7c, bottom panel). It is possible that the precipitation centroid moved southeast around the central $\delta^{18}O$ site as there is evidence for wetter conditions to the southeast (Whitney et al., 2011; Fornace et al., 2016) and drier conditions to the north (Deplazes et al., 2013; Zular et al., 2019), as well as some evidence for a south-shift of the energy flux equator (Arbuszewski et al., 2013). The southeast appears to become drier around 12 ka, approximately when a nearby speleothem $\delta^{18}O$ shift occurs that is consistent with decreased Amazon and more Atlantic-derived moisture (Fig. S8) (Novello et al., 2017, 2018).

As the precipitation centroid migrates further east, after ∼12 ka, pollen data from semi-arid northeastern Brazil (near the eastern $\delta^{18}O$ site) suggest humid conditions from ∼10.9-6.7 ka (De Oliveira et al., 1999). Humidity peaks halfway through this interval (∼8.9 ka) when eastern $\delta^{18}O$ reaches its lowest values (De Oliveira et al., 1999; Cruz et al., 2009), suggesting this marks the easternmost extent and turning point of the precipitation centroid. As discussed earlier, this timing also corresponds with the onset of

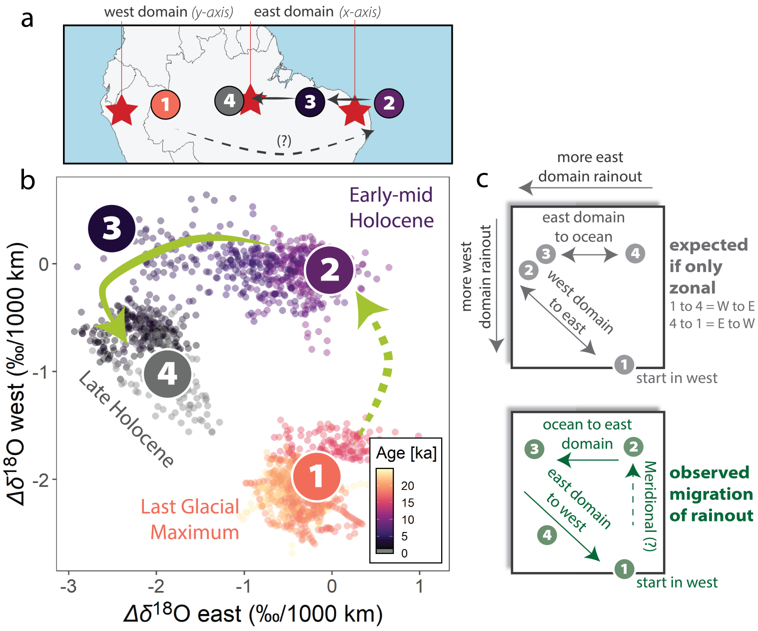

Figure 7. Isotope gradients reflect zonal and meridional shifts in monsoon precipitation centroid. (**A**) Map of speleothem sites showing the east and west domains—the axes of panel B—and a schematic for the interpretation of panel B. (**B**) Crossplot of eastern and western domain data. Points correspond with numbers in panels A and C. (**C**) More negative $\Delta\delta^{18}O$ refers to more rainout in a given domain. Data should track a sideways "V" shape if the focus of rainout migrates only zonally (top panel, note different order of numbers). However, the LGM to early-mid Holocene does not follow this zonal trajectory, suggesting a meridional component (dashed arrow).

the time-transgressive westward shift in wet conditions that continues to the present. While more work is needed to trace the past focus of Amazon rainfall, we suggest the progressive shifts in wet conditions across the continent (both east-west and west-east) provide empirical support and a testable framework for the pattern of monsoon migration.

5.4 Mechanisms for zonal monsoon migration

While climate model simulations are necessary to assess the dynamical drivers of monsoon migration, our analysis allows us to present testable hypotheses. For example, the greening of the Sahara at the mid-Holocene (about 70 W/m^2 anomalous heat source at top of atmosphere; Boos and Korty (2016)) is likely sufficient to drive the monsoon's energy flux prime meridian eastward entirely over the tropical Atlantic (Fig. 6e, f). Comparison to proxy records from Africa generally support this remote influence on the South American Monsoon. Dust flux records of West African Monsoon behavior show pronounced precession-scale variability in the last 240 kyr with prominent exceptions at ∼30, ∼70, and ∼150 ka when dust fluxes "skip" precession beats (Skonieczny et al., 2019). In South America, western Amazon $\delta^{18}O$ records lose sensitivity to precession at the same times (and $\Delta\delta^{18}O$ where there is data, in the ∼30 ka case; Fig. S7, inset) (Mosblech et al., 2012; Cheng et al., 2013; Wang et al., 2017). Travertine deposits from northeast Brazil support the precession-pacing of the SAPD and also show a skipped beat at ∼150 ka (Wang et al., 2004). Further, there is a rapid increase in $\delta^{18}O$ at the eastern site at ∼5 ka, consistent with a westward (inland) shift of rainout, contemporaneous with the termination of the African Humid Period in North Africa (Shanahan et al., 2015) where increasing land albedo would provide an anomalous energy sink. These similarities are mostly preliminary and more data is needed to test if they hold over space and time, but they are consistent with expectations if the zonal location of the South American Monsoon was sensitive to Saharan albedo.

At the LGM, vegetation change that increases land albedo in tropical Africa and Eurasia could push the energy flux prime meridian westward. However, it is not clear if the magnitude of forcing required for this shift could be accomplished by the LGM vegetation change alone. For example, low $\Delta\delta^{18}O$ values (along with high runoff (Nace et al., 2014)) are a persistent feature in the western domain for at least ~20 kyr before the LGM (Fig. S7, inset), suggesting the cause of a westward shift in rainout is not unique to this time interval. African dust fluxes were persistently high from 40-20 ka, consistent with a remote albedo forcing, but data for other possible drivers monsoon migration, such as the strength of the easterlies, is sparse at this time.

Based on the zonal, meridional, and hysteresis-like migration of the focus of South American Monsoon rainout, we suggest that multiple forcing mechanisms operate at different times to drive complex patterns of monsoon migration. Our analysis suggests that remote land albedo change could drive the zonal patterns of monsoon rainout, and some features of the proxy data support such a trans-Atlantic correlation, but more sophisticated climate model simulations are needed to rigorously test these hypotheses.

6 Limitations and future directions

Our analysis provides a path forward for resolving the enigmatic, non-uniform trends in tropical South American speleothem $\delta^{18}O$, but it rests on assumptions, many previously discussed, that deserve further scrutiny. One critical assumption that is difficult to address is that speleothem $\delta^{18}O$ reliably tracks precipitation $\delta^{18}O$ at all sites. Kinetic fractionation and other confounding processes could decouple speleothem and precipitation $\delta^{18}O$, challenging our model approach. Such effects have not been documented in these speleothem (van Breukelen et al., 2008; Cruz et al., 2009; Cheng et al., 2013; Wang et al., 2017), but additional proxy constraints (such as triple oxygen and mass-48 clumped isotopes) will provide more rigorous tests of local and kinetic effects (Huth et al., 2022). Another limitation lies in our simplified monsoon energy balance modeling approach. The goal of these model exercises is to present plausible drivers of zonal monsoon shifts for further testing, while recognizing that our list is not exhaustive. Future Earth System Modeling studies of the SAPD should analyze the zonal location of the energy flux prime meridian and its relation to zonal precipitation patterns to test whether this zonal monsoon migration effect is present.

We argue that zonal monsoon migration explains the late Quaternary SAPD, but similar zonal precipitation anomalies at other times in the past could be related to different dynamics. As stated earlier, the SAPD is an empirical rainfall pattern that appears on precession (Martin et al., 1997; Cruz et al., 2009; Liu & Battisti, 2015) and glacial-interglacial timescales (Abouchami & Zabel, 2003; Mason et al., 2019), and its underlying cause likely varies with time. Changes in monsoon strength and its associated circulation can also cause zonal precipitation anomalies (Cruz et al., 2009; Liu & Battisti, 2015), albeit likely at a lower amplitude than we estimate for the late Quaternary. At present, our understanding of what causes zonal monsoon migration in South America (or elsewhere) is limited, so we cannot know how pervasive this dynamic might be in paleoclimate records. However, our results support previous work (Battisti et al., 2014) suggesting that zonal forcings may help explain some of the enigmatic proxy records found in places where monsoons are energetically primed to migrate east-west.

Data Availability Statement

Code and data associated with this study can be found through Zenodo (Kukla et al., 2022) and Github (`https://github.com/tykukla/ZonalPrecipPatterns-Amazon`). The Zenodo/Github repository includes code and results for the energy balance and reactive transport model analysis, SISALv2 analysis, Amazon speleothem $\delta^{18}O$ data cleaning and smoothing, and the proxy compilation in Figure 1 of the main text. We note that the Tigre Perdido record (van Breukelen et al., 2008) from the western composite data was downloaded from the SISAL database (siteID: 25), while other speleothem records were provided by the original authors or taken from the supplementary materials of the relevant publication.

Acknowledgments

We thank F. W. Cruz, J. K. C. Rugenstein, W. Boos, and C. Skinner for thoughtful discussion. We also thank F. W. Cruz, X. Wang, and H. Cheng for sharing the speleothem data used in this study. We thank S. J. Burns for helpful comments on an earlier version of this manuscript. We acknowledge the SISAL (Speleothem Isotopes Synthesis and Analysis) working group and data contributors. SISAL is a working group of the Past Global Changes (PAGES) programme. We acknowledge the World Climate Research Programme's Working Group on Coupled Modelling, which is responsible for CMIP, and we thank the climate modeling groups for producing and making available their model output. For CMIP the U.S. Department of Energy's Program for Climate Model Diagnosis and Intercomparison provides coordinating support and led development of software infrastructure in partnership with the Global Organization for Earth System Science Portals. We thank developers and providers of all data sources used in this study including GPCCv8, NCEP Reanalysis 2, GNIP, and PMIP3/CMIP5. NCEP_Reanalysis 2 data provided by the NOAA/OAR/ESRL PSD, Boulder, Colorado, USA from their web site at https://www.esrl.noaa.gov/psd. T. K. acknowledges support from the Stanford McGee/Levorsen research grant. The authors declare no competing interests.

References

Abouchami, W., & Zabel, M. (2003, August). Climate forcing of the Pb isotope record of terrigenous input into the Equatorial Atlantic. *Earth and Planetary Science Letters*, *213*(3-4), 221–234. doi: 10.1016/S0012-821X(03)00304-2

Adam, O., Bischoff, T., & Schneider, T. (2016, October). Seasonal and Interannual Variations of the Energy Flux Equator and ITCZ. Part II: Zonally Varying Shifts of the ITCZ. *Journal of Climate*, *29*(20), 7281–7293. doi: 10.1175/JCLI-D-15-0710.1

Adkins, J., deMenocal, P., & Eshel, G. (2006, December). The "African humid period" and the record of marine upwelling from excess ^{230} Th in Ocean Drilling Program Hole 658C. *Paleoceanography*, *21*(4), PA4203. doi: 10.1029/2005PA001200

Ampuero, A., Stríkis, N. M., Apaéstegui, J., Vuille, M., Novello, V. F., Espinoza, J. C., ... Sifeddine, A. (2020, February). The Forest Effects on the Isotopic Composition of Rainfall in the Northwestern Amazon Basin. *Journal of Geophysical Research: Atmospheres*, *125*(4). doi: 10.1029/2019JD031445

Arbuszewski, J. A., deMenocal, P. B., Cléroux, C., Bradtmiller, L., & Mix, A. (2013, November). Meridional shifts of the Atlantic intertropical convergence zone since the Last Glacial Maximum. *Nature Geoscience*, *6*(11), 959–962. doi: 10.1038/ngeo1961

Arz, H. W., Pätzold, J., & Wefer, G. (1998). Correlated Millennial-Scale Changes in Surface Hydrography and Terrigenous Sediment Yield Inferred from Last-Glacial Marine Deposits off Northeastern Brazil. *Quaternary Research*, *50*, 157–166.

Arz, H. W., Pätzold, J., & Wefer, G. (1999, December). Climatic changes during the last deglaciation recorded in sediment cores from the northeastern Brazilian Continental Margin. *Geo-Marine Letters*, *19*(3), 209–218. doi: 10.1007/s003670050111

Atsawawaranunt, K., Comas-Bru, L., Mozhdehi, S. A., Deininger, M., Harrison, S. P., Baker, A., … Scroxton, N. (2018). The SISAL database: A global resource to document oxygen and carbon isotope records from speleothems. *Earth System Science Data*, *10*, 1687–1713.

Baker, J. C. A., Gloor, M., Spracklen, D. V., Arnold, S. R., Tindall, J. C., Clerici, S. J., … Brienen, R. J. W. (2016, November). What drives interannual variation in tree ring oxygen isotopes in the Amazon?: WHAT DRIVES AMAZON TREE RING δ^{18}O? *Geophysical Research Letters*, *43*(22), 11,831–11,840. doi: 10.1002/2016GL071507

Baker, P. A., Rigsby, C. A., Seltzer, G. O., Fritz, S. C., Lowenstein, T. K., Bacher, N. P., & Veliz, C. (2001, February). Tropical climate changes at millennial and orbital timescales on the Bolivian Altiplano. *Nature*, *409*(6821), 698–701. doi: 10.1038/35055524

Baker, P. A., Seltzer, G. O., Fritz, S. C., Dunbar, R. B., Grove, M. J., Tapia, P. M., … Broda, J. P. (2001, January). The History of South American Tropical Precipitation for the Past 25,000 Years. *Science*, *291*(5504), 640–643. doi: 10.1126/science.291.5504.640

Battisti, D. S., Ding, Q., & Roe, G. H. (2014, November). Coherent pan-Asian climatic and isotopic response to orbital forcing of tropical insolation. *Journal of Geophysical Research: Atmospheres*, *119*(21), 11,997–12,020. doi: 10.1002/2014JD021960

Behling, H., Arz, H. W., Pätzold, J., & Wefer, G. (2002, May). Late Quaternary vegetational and climate dynamics in southeastern Brazil, inferences from marine cores GeoB 3229-2 and GeoB 3202-1. *Palaeogeography, Palaeoclimatology, Palaeoecology*, *179*(3-4), 227–243. doi: 10.1016/S0031-0182(01)00435-7

Binney, H., Edwards, M., Macias-Fauria, M., Lozhkin, A., Anderson, P., Kaplan, J. O., … Zernitskaya, V. (2017, February). Vegetation of Eurasia from the last glacial maximum to present: Key biogeographic patterns. *Quaternary Science Reviews*, *157*, 80–97. doi: 10.1016/j.quascirev.2016.11.022

Boers, N., Rheinwalt, A., Bookhagen, B., Barbosa, H. M. J., Marwan, N., Marengo, J., & Kurths, J. (2014, October). The South American rainfall dipole: A complex network analysis of extreme events: BOERS ET AL. *Geophysical Research Letters*, *41*(20), 7397–7405. doi: 10.1002/2014GL061829

Boos, W. R., & Korty, R. L. (2016, December). Regional energy budget control of the intertropical convergence zone and application to mid-Holocene rainfall. *Nature Geoscience*, *9*(12), 892–897. doi: 10.1038/ngeo2833

Bradtmiller, L. I., McGee, D., Awalt, M., Evers, J., Yerxa, H., Kinsley, C. W., & deMenocal, P. B. (2016, January). Changes in biological productivity along the northwest African margin over the past 20,000 years. *Paleoceanography*, *31*(1), 185–202. doi: 10.1002/2015PA002862

Brienen, R. J. W., Helle, G., Pons, T. L., Guyot, J.-l., & Gloor, M. (2012). Oxygen isotopes in tree rings are a good proxy for Amazon precipitation and El Niño-Southern Oscillation variability. *Proceedings of the National Academy of Sciences*, *109*(42). doi: 10.1073/pnas.1205977109

Brierley, C., & Wainer, I. (2018, October). Inter-annual variability in the tropical Atlantic from the Last Glacial Maximum into future climate projections simulated by CMIP5/PMIP3. *Climate of the Past*, *14*(10), 1377–1390. doi: 10.5194/cp-14-1377-2018

Campos, M. C., Chiessi, C. M., Prange, M., Mulitza, S., Kuhnert, H., Paul, A., … Bahr, A. (2019, December). A new mechanism for millennial scale positive precipitation anomalies over tropical South America. *Quaternary Science*

Reviews, *225*, 105990. doi: 10.1016/j.quascirev.2019.105990

Caves, J. K., Winnick, M. J., Graham, S. A., Sjostrom, D. J., Mulch, A., & Chamberlain, C. P. (2015). Role of the westerlies in Central Asia climate over the Cenozoic. *Earth and Planetary Science Letters*, *428*, 33–43. doi: 10.1016/j.epsl.2015.07.023

Chamberlain, C. P., Winnick, M. J., Mix, H. T., Chamberlain, S. D., & Maher, K. (2014). The impact of neogene grassland expansion and aridification on the isotopic composition of continental precipitation. *Global Biogeochemical Cycles*, *28*(9), 992–1004. doi: 10.1002/2014GB004822

Cheng, H., Sinha, A., Cruz, F. W., Wang, X., Edwards, R. L., D'Horta, F. M., ... Auler, A. S. (2013). Climate change patterns in Amazonia and biodiversity. *Nature Communications*, *4*, 1–6. doi: 10.1038/ncomms2415

Comas-Bru, L., Harrison, S. P., Werner, M., Rehfeld, K., Scroxton, N., Veiga-Pires, C., & SISAL working group members. (2019, August). Evaluating model outputs using integrated global speleothem records of climate change since the last glacial. *Climate of the Past*, *15*(4), 1557–1579. doi: 10.5194/cp-15-1557-2019

Comas-Bru, L., Rehfeld, K., Roesch, C., Amirnezhad-Mozhdehi, S., Harrison, S. P., Atsawawaranunt, K., ... SISAL Working Group members (2020, October). SISALv2: A comprehensive speleothem isotope database with multiple age–depth models. *Earth System Science Data*, *12*(4), 2579–2606. doi: 10.5194/essd-12-2579-2020

Cruz, F. W., Vuille, M., Burns, S. J., Wang, X., Cheng, H., Werner, M., ... Nguyen, H. (2009, March). Orbitally driven east–west antiphasing of South American precipitation. *Nature Geoscience*, *2*(3), 210–214. doi: 10.1038/ngeo444

Dee, S., Noone, D., Buenning, N., Emile-Geay, J., & Zhou, Y. (2015, January). SPEEDY-IER: A fast atmospheric GCM with water isotope physics. *Journal of Geophysical Research: Atmospheres*, *120*(1), 73–91. doi: 10.1002/2014JD022194

De Oliveira, P. E., Barreto, A. M. F., & Suguio, K. (1999, September). Late Pleistocene/Holocene climatic and vegetational history of the Brazilian caatinga: The fossil dunes of the middle São Francisco River. *Palaeogeography, Palaeoclimatology, Palaeoecology*, *152*(3-4), 319–337. doi: 10.1016/S0031-0182(99)00061-9

Deplazes, G., Lückge, A., Peterson, L. C., Timmermann, A., Hamann, Y., Hughen, K. A., ... Haug, G. H. (2013, March). Links between tropical rainfall and North Atlantic climate during the last glacial period. *Nature Geoscience*, *6*(3), 213–217. doi: 10.1038/ngeo1712

Ford, H. L., McChesney, C. L., Hertzberg, J. E., & McManus, J. F. (2018, November). A Deep Eastern Equatorial Pacific Thermocline During the Last Glacial Maximum. *Geophysical Research Letters*, *45*(21). doi: 10.1029/2018GL079710

Fornace, K. L., Whitney, B. S., Galy, V., Hughen, K. A., & Mayle, F. E. (2016, March). Late Quaternary environmental change in the interior South American tropics: New insight from leaf wax stable isotopes. *Earth and Planetary Science Letters*, *438*, 75–85. doi: 10.1016/j.epsl.2016.01.007

Fritz, S. C., Baker, P. A., Lowenstein, T. K., Seltzer, G. O., Rigsby, C. A., Dwyer, G. S., ... Luo, S. (2004, January). Hydrologic variation during the last 170,000 years in the southern hemisphere tropics of South America. *Quaternary Research*, *61*(01), 95–104. doi: 10.1016/j.yqres.2003.08.007

Gat, J. R., & Matsui, E. (1991). Atmospheric water balance in the Amazon basin: An isotopic evapotranspiration model. *Journal of Geophysical Research*, *96*(D7), 13179. doi: 10.1029/91JD00054

Grootes, P. M., Stuiver, M., Thompson, L. G., & Mosley-Thompson, E. (1989). Oxygen isotope changes in tropical ice, Quelccaya, Peru. *Journal of Geophysi-*

cal Research, *94*(D1), 1187. doi: 10.1029/JD094iD01p01187

Gu, F., Zonneveld, K. A., Chiessi, C. M., Arz, H. W., Pätzold, J., & Behling, H. (2017, September). Long-term vegetation, climate and ocean dynamics inferred from a 73,500 years old marine sediment core (GeoB2107-3) off southern Brazil. *Quaternary Science Reviews*, *172*, 55–71. doi: 10.1016/j.quascirev.2017.06.028

Häggi, C., Chiessi, C. M., Merkel, U., Mulitza, S., Prange, M., Schulz, M., & Schefuß, E. (2017, December). Response of the Amazon rainforest to late Pleistocene climate variability. *Earth and Planetary Science Letters*, *479*, 50–59. doi: 10.1016/j.epsl.2017.09.013

Hu, C., Henderson, G. M., Huang, J., Xie, S., Sun, Y., & Johnson, K. R. (2008, February). Quantification of Holocene Asian monsoon rainfall from spatially separated cave records. *Earth and Planetary Science Letters*, *266*(3-4), 221–232. doi: 10.1016/j.epsl.2007.10.015

Huth, T. E., Passey, B. H., Cole, J. E., Lachniet, M. S., McGee, D., Denniston, R. F., . . . Levin, N. E. (2022, February). A framework for triple oxygen isotopes in speleothem paleoclimatology. *Geochimica et Cosmochimica Acta*, *319*, 191–219. doi: 10.1016/j.gca.2021.11.002

Jaeschke, A., Rühlemann, C., Arz, H., Heil, G., & Lohmann, G. (2007, December). Coupling of millennial-scale changes in sea surface temperature and precipitation off northeastern Brazil with high-latitude climate shifts during the last glacial period: TROPICAL-POLAR ATLANTIC CLIMATE COUPLING. *Paleoceanography*, *22*(4), PA4206. doi: 10.1029/2006PA001391

Keys, P. W., van der Ent, R. J., Gordon, L. J., Hoff, H., Nikoli, R., & Savenije, H. H. G. (2012, February). Analyzing precipitationsheds to understand the vulnerability of rainfall dependent regions. *Biogeosciences*, *9*(2), 733–746. doi: 10.5194/bg-9-733-2012

Konecky, B. L., Noone, D. C., & Cobb, K. M. (2019, February). The Influence of Competing Hydroclimate Processes on Stable Isotope Ratios in Tropical Rainfall. *Geophysical Research Letters*, *46*(3), 1622–1633. doi: 10.1029/2018GL080188

Koutavas, A., & Joanides, S. (2012, December). El Niño-Southern Oscillation extrema in the Holocene and Last Glacial Maximum: ENSO EXTREMA IN THE HOLOCENE AND LGM. *Paleoceanography*, *27*(4). doi: 10.1029/2012PA002378

Kukla, T., Ahlström, A., Maezumi, S. Y., Chevalier, M., Lu, Z., Winnick, M. J., & Chamberlain, C. P. (2021, July). The resilience of Amazon tree cover to past and present drying. *Global and Planetary Change*, *202*, 103520. doi: 10.1016/j.gloplacha.2021.103520

Kukla, T., Winnick, M. J., Laguë, M. M., & Xia, Z. (2022). Project files, data, and code. *Zenodo*. doi: 10.5281/zenodo.6618194

Kukla, T., Winnick, M. J., Maher, K., Ibarra, D. E., & Chamberlain, C. P. (2019, January). The Sensitivity of Terrestrial δ^{18}O Gradients to Hydroclimate Evolution. *Journal of Geophysical Research: Atmospheres*, *124*, 563–582. doi: 10.1029/2018JD029571

Lee, J.-E., Johnson, K., & Fung, I. (2009). Precipitation over South America during the Last Glacial Maximum: An analysis of the "amount effect" with a water isotope-enabled general circulation model. *Geophysical Research Letters*, *36*(19), L19701. doi: 10.1029/2009GL039265

Liu, X., & Battisti, D. S. (2015, June). The Influence of Orbital Forcing of Tropical Insolation on the Climate and Isotopic Composition of Precipitation in South America. *Journal of Climate*, *28*(12), 4841–4862. doi: 10.1175/JCLI-D-14-00639.1

Lu, Z., Zhang, Q., Miller, P. A., Zhang, Q., Berntell, E., & Smith, B. (2021, January). Impacts of Large-Scale Sahara Solar Farms on Global Climate and Vegetation Cover. *Geophysical Research Letters*, *48*(2). doi: 10.1029/2020GL090789

Marengo, J. A., Alves, L. M., Soares, W. R., Rodriguez, D. A., Camargo, H., Riveros, M. P., & Pabló, A. D. (2013, November). Two Contrasting Severe Seasonal Extremes in Tropical South America in 2012: Flood in Amazonia and Drought in Northeast Brazil. *Journal of Climate*, *26*(22), 9137–9154. doi: 10.1175/JCLI-D-12-00642.1

Martin, L., Bertaux, J., Corrège, T., Ledru, M.-P., Mourguiart, P., Sifeddine, A., ... Turcq, B. (1997, January). Astronomical Forcing of Contrasting Rainfall Changes in Tropical South America between 12,400 and 8800 cal yr B.P. *Quaternary Research*, *47*(1), 117–122. doi: 10.1006/qres.1996.1866

Mason, C. C., Romans, B. W., Stockli, D. F., Mapes, R. W., & Fildani, A. (2019, June). Detrital zircons reveal sea-level and hydroclimate controls on Amazon River to deep-sea fan sediment transfer. *Geology*, *47*(6), 563–567. doi: 10.1130/G45852.1

McGee, D., deMenocal, P., Winckler, G., Stuut, J., & Bradtmiller, L. (2013, June). The magnitude, timing and abruptness of changes in North African dust deposition over the last 20,000yr. *Earth and Planetary Science Letters*, *371–372*, 163–176. doi: 10.1016/j.epsl.2013.03.054

McIntyre, A., & Molfino, B. (1996, December). Forcing of Atlantic Equatorial and Subpolar Millennial Cycles by Precession. *Science*, *274*(5294), 1867–1870. doi: 10.1126/science.274.5294.1867

Mosblech, N. A. S., Bush, M. B., Gosling, W. D., Hodell, D., Thomas, L., van Calsteren, P., ... van Woesik, R. (2012, November). North Atlantic forcing of Amazonian precipitation during the last ice age. *Nature Geoscience*, *5*(11), 817–820. doi: 10.1038/ngeo1588

Mulitza, S., Chiessi, C. M., Schefuß, E., Lippold, J., Wichmann, D., Antz, B., ... Zhang, Y. (2017, June). Synchronous and proportional deglacial changes in Atlantic meridional overturning and northeast Brazilian precipitation: AMOC and Precipitation over NE Brazil. *Paleoceanography*, *32*(6), 622–633. doi: 10.1002/2017PA003084

Nace, T. E., Baker, P. A., Dwyer, G. S., Silva, C. G., Rigsby, C. A., Burns, S. J., ... Zhu, J. (2014, December). The role of North Brazil Current transport in the paleoclimate of the Brazilian Nordeste margin and paleoceanography of the western tropical Atlantic during the late Quaternary. *Palaeogeography, Palaeoclimatology, Palaeoecology*, *415*, 3–13. doi: 10.1016/j.palaeo.2014.05.030

Nogués-Paegle, J., & Mo, K. C. (1997, February). Alternating Wet and Dry Conditions over South America during Summer. *Monthly Weather Review*, *125*(2), 279–291. doi: 10.1175/1520-0493(1997)125⟨0279:AWADCO⟩2.0.CO;2

Novello, V. F., Cruz, F. W., Moquet, J. S., Vuille, M., de Paula, M. S., Nunes, D., ... Campos, J. L. P. S. (2018, May). Two Millennia of South Atlantic Convergence Zone Variability Reconstructed From Isotopic Proxies. *Geophysical Research Letters*, *45*(10), 5045–5051. doi: 10.1029/2017GL076838

Novello, V. F., Cruz, F. W., Vuille, M., Stríkis, N. M., Edwards, R. L., Cheng, H., ... Santos, R. V. (2017, December). A high-resolution history of the South American Monsoon from Last Glacial Maximum to the Holocene. *Scientific Reports*, *7*(1). doi: 10.1038/srep44267

Pattnayak, K., Tindall, J., Brienen, R., Barichivich, J., & Gloor, E. (2019, October). Can we detect changes in Amazon forest structure using measurements of the isotopic composition of precipitation? *Geophysical Research Letters*, *46*. doi: 10.1029/2019GL084749

Prentice, I. C., Harrison, S. P., & Bartlein, P. J. (2011, March). Global vegetation and terrestrial carbon cycle changes after the last ice age. *New Phytologist*, *189*(4), 988–998. doi: 10.1111/j.1469-8137.2010.03620.x

Reis, L. S., Guimarães, J. T. F., Souza-Filho, P. W. M., Sahoo, P. K., de

Figueiredo, M. M. J. C., de Souza, E. B., & Giannini, T. C. (2017, August). Environmental and vegetation changes in southeastern Amazonia during the late Pleistocene and Holocene. *Quaternary International*, *449*, 83–105. doi: 10.1016/j.quaint.2017.04.031

Salati, E., Dall'Olio, A., Matsui, E., & Gat, J. R. (1979). Recycling of water in the Amazon Basin: An isotopic study. *Water Resources Research*, *15*(5), 1250–1258. doi: 10.1029/WR015i005p01250

Scheff, J., & Frierson, D. M. W. (2014). Scaling potential evapotranspiration with greenhouse warming. *Journal of Climate*, *27*(4), 1539–1558. doi: 10.1175/JCLI-D-13-00233.1

Shanahan, T. M., McKay, N. P., Hughen, K. A., Overpeck, J. T., Otto-Bliesner, B., Heil, C. W., … Peck, J. (2015, February). The time-transgressive termination of the African Humid Period. *Nature Geoscience*, *8*(2), 140–144. doi: 10.1038/ngeo2329

Sherwood, S. C., Ingram, W., Tsushima, Y., Satoh, M., Roberts, M., Vidale, P. L., & O'Gorman, P. A. (2010, May). Relative humidity changes in a warmer climate. *Journal of Geophysical Research*, *115*(D9), D09104. doi: 10.1029/2009JD012585

Shimizu, M. H., Sampaio, G., Venancio, I. M., & Maksic, J. (2020, January). Seasonal changes of the South American monsoon system during the Mid-Holocene in the CMIP5 simulations. *Climate Dynamics*. doi: 10.1007/s00382-020-05137-1

Siler, N., Roe, G. H., Armour, K. C., & Feldl, N. (2019, April). Revisiting the surface-energy-flux perspective on the sensitivity of global precipitation to climate change. *Climate Dynamics*, *52*(7-8), 3983–3995. doi: 10.1007/s00382-018-4359-0

Skonieczny, C., McGee, D., Winckler, G., Bory, A., Bradtmiller, L. I., Kinsley, C. W., … Malaizé, B. (2019, January). Monsoon-driven Saharan dust variability over the past 240,000 years. *Science Advances*, *5*(1), eaav1887. doi: 10.1126/sciadv.aav1887

Tapia, P. M., Fritz, S. C., Baker, P. A., Seltzer, G. O., & Dunbar, R. B. (2003, May). A Late Quaternary diatom record of tropical climatic history from Lake Titicaca (Peru and Bolivia). *Palaeogeography, Palaeoclimatology, Palaeoecology*, *194*(1-3), 139–164. doi: 10.1016/S0031-0182(03)00275-X

van Breukelen, M., Vonhof, H., Hellstrom, J., Wester, W., & Kroon, D. (2008, October). Fossil dripwater in stalagmites reveals Holocene temperature and rainfall variation in Amazonia. *Earth and Planetary Science Letters*, *275*(1-2), 54–60. doi: 10.1016/j.epsl.2008.07.060

van der Ent, R. J., Wang-Erlandsson, L., Keys, P. W., & Savenije, H. H. G. (2014, December). Contrasting roles of interception and transpiration in the hydrological cycle – Part 2: Moisture recycling. *Earth System Dynamics*, *5*(2), 471–489. doi: 10.5194/esd-5-471-2014

Venancio, I. M., Mulitza, S., Govin, A., Santos, T. P., Lessa, D. O., Albuquerque, A. L. S., … Schulz, M. (2018, December). Millennial- to Orbital-Scale Responses of Western Equatorial Atlantic Thermocline Depth to Changes in the Trade Wind System Since the Last Interglacial. *Paleoceanography and Paleoclimatology*, *33*(12), 1490–1507. doi: 10.1029/2018PA003437

Vimeux, F., Gallaire, R., Bony, S., Hoffmann, G., & Chiang, J. (2005, December). What are the climate controls on δD in precipitation in the Zongo Valley (Bolivia)? Implications for the Illimani ice core interpretation. *Earth and Planetary Science Letters*, *240*(2), 205–220. doi: 10.1016/j.epsl.2005.09.031

Vuille, M., Bradley, R. S., Werner, M., Healy, R., & Keimig, F. (2003). Modeling δ18O in precipitation over the tropical Americas: 1. Interannual variability and climatic controls. *Journal of Geophysical Research: Atmospheres*, *108*(D6). doi: 10.1029/2001JD002038

Vuille, M., & Werner, M. (2005). Stable isotopes in precipitation recording South American summer monsoon and ENSO variability: Observations and model results. *Climate Dynamics*, *25*(4), 401–413. doi: 10.1007/s00382-005-0049-9

Wang, X., Auler, A. S., Edwards, R. L., Cheng, H., Cristalli, P. S., Smart, P. L., ... Shen, C.-C. (2004, December). Wet periods in northeastern Brazil over the past 210 kyr linked to distant climate anomalies. *Nature*, *432*(7018), 740–743. doi: 10.1038/nature03067

Wang, X., Edwards, R. L., Auler, A. S., Cheng, H., Kong, X., Wang, Y., ... Chiang, H.-W. (2017, January). Hydroclimate changes across the Amazon lowlands over the past 45,000 years. *Nature*, *541*(7636), 204–207. doi: 10.1038/nature20787

Ward, B. M., Wong, C. I., Novello, V. F., McGee, D., Santos, R. V., Silva, L. C., ... Cheng, H. (2019, April). Reconstruction of Holocene coupling between the South American Monsoon System and local moisture variability from speleothem δ18O and 87Sr/86Sr records. *Quaternary Science Reviews*, *210*, 51–63. doi: 10.1016/j.quascirev.2019.02.019

Whitney, B. S., Mayle, F. E., Punyasena, S. W., Fitzpatrick, K. A., Burn, M. J., Guillen, R., ... Metcalfe, S. E. (2011, July). A 45kyr palaeoclimate record from the lowland interior of tropical South America. *Palaeogeography, Palaeoclimatology, Palaeoecology*, *307*(1-4), 177–192. doi: 10.1016/j.palaeo.2011.05.012

Winnick, M. J., Chamberlain, C. P., Caves, J. K., & Welker, J. M. (2014). Quantifying the isotopic 'continental effect'. *Earth and Planetary Science Letters*, *406*, 123–133. doi: 10.1016/j.epsl.2014.09.005

Worden, Noone, D., Bowman, K., & Tropospheric Emission Spectrometer science team and data. (2007, February). Importance of rain evaporation and continental convection in the tropical water cycle. *Nature*, *445*(7127), 528–532. doi: 10.1038/nature05508

Wortham, B. E., Wong, C. I., Silva, L. C., McGee, D., Montañez, I. P., Troy Rasbury, E., ... Santos, R. V. (2017, April). Assessing response of local moisture conditions in central Brazil to variability in regional monsoon intensity using speleothem 87Sr/86Sr values. *Earth and Planetary Science Letters*, *463*, 310–322. doi: 10.1016/j.epsl.2017.01.034

Wu, H., Guiot, J., Brewer, S., & Guo, Z. (2007, June). Climatic changes in Eurasia and Africa at the last glacial maximum and mid-Holocene: Reconstruction from pollen data using inverse vegetation modelling. *Climate Dynamics*, *29*(2-3), 211–229. doi: 10.1007/s00382-007-0231-3

Zheng, W., Braconnot, P., Guilyardi, E., Merkel, U., & Yu, Y. (2008, June). ENSO at 6ka and 21ka from ocean–atmosphere coupled model simulations. *Climate Dynamics*, *30*(7-8), 745–762. doi: 10.1007/s00382-007-0320-3

Zular, A., Sawakuchi, A. O., Chiessi, C. M., d'Horta, F. M., Cruz, F. W., Demattê, J. A. M., ... Soares, E. A. A. (2019, January). The role of abrupt climate change in the formation of an open vegetation enclave in northern Amazonia during the late Quaternary. *Global and Planetary Change*, *172*, 140–149. doi: 10.1016/j.gloplacha.2018.09.006